CrystEngComm

Accepted Manuscript

ROYAL SOCIETY OF CHEMISTRY

www.rsc.org/crystengcomm

Modeling of Strontium Chloride Hexahydrate Growth during Unseeded Batch Cooling Crystallization by Two-Dimensional Population Balance Equation

Yuanyuan Qian[a], Guimin Lu[*a], Yuzhu Sun[a], Xingfu Song[a], Jianguo Y[a]

Abstract: In this study, the growth of strontium chloride hexahydrate during unseeded batch cooling crystallization was investigated and modeled by the two-dimensional population balance equation. The results suggested that in a well-mixed crystallizer, no obvious agglomeration and breakage were observed. The initial supersaturation and cooling rate were the key factors of crystal growth and the crystals grew following a size dependent mechanism. Thus, the growth of $SrCl_2 \cdot 6H_2O$ was modeled as a function of supersaturation, temperature, and crystal size. The calculated crystal size and size distribution showed a good agreement with the experimental ones, proving the model could well predict the growth behavior of $SrCl_2 \cdot 6H_2O$ in the system. This study not only fills the research vacancy of $SrCl_2 \cdot 6H_2O$ crystallization, but also contributes to the optimal design of the crystallization process, aiming at preparing $SrCl_2 \cdot 6H_2O$ crystals with a larger size and a narrower size distribution.

Keywords: strontium chloride hexahydrate; batch cooling crystallization, crystal growth model; two-dimensional balance equation

* Corresponding author. Phone/Fax: +86-21-64252065. *E-mail address*: gmlu@ecust.edu.cn

[a] National Engineering Research Center for Integrated Utilization of Salt Lake Resources, East China University of Science and Technology, Shanghai, 200237, China

1 INTRODUCTION

Strontium chloride hexahydrate ($SrCl_2 \cdot 6H_2O$) is an important raw material for electrolysis, pharmacy, and pyrotechnics industry. $SrCl_2 \cdot 6H_2O$ is usually prepared by a batch-cooling crystallization, and the shape of $SrCl_2 \cdot 6H_2O$ crystals obtained is fine needle-like [1, 2]. The crystals in this shape are not good for easy downstream operations which require such properties as excellent filterability, low fine concentrations, low trend to cake on storage, good flowing ability, etc. Therefore, to prepare $SrCl_2 \cdot 6H_2O$ crystals with a larger size and a narrower size distribution becomes a real challenge in the research on the $SrCl_2 \cdot 6H_2O$ crystallization. However, it has been rarely reported as yet.

The multidimensional crystal size and size distribution are determined by the growth rates along different growth directions. During a batch-cooling crystallization process, several operational factors affect the crystal growth. In our reported study, the effects of initial supersaturation, cooling rate, stirring rate, aging time, and seed addition on the $SrCl_2 \cdot 6H_2O$ growth were investigated. The results indicated that in a well-mixed batch $SrCl_2 \cdot 6H_2O$ crystallizer, initial supersaturation and cooling rate were the key factors of crystal growth rate, significantly affecting the crystal size and size distribution, whereas stirring rate and aging time were undistinguished factors. The addition of small seeds in an appropriate amount was beneficial to a narrow crystal size distribution; however, it led to a decreasing in crystal size, which might be undesirable. In conclusion, under a stirring rate of 450 rpm and an aging time of 10 min, an optimal operation range was suggested with an initial supersaturation ratio of 1.150~1.250, a cooling rate of 15.0~20 °C·h^{-1}. The as-prepared $SrCl_2 \cdot 6H_2O$ crystals were long

rod-like with an average length (L_{mean}) of 1206.78 μm and an average width (W_{mean}) of 80.06 μm. The crystals had a relatively narrow size distribution with the coefficient of length variation ($C.V._L$) in 0.2372 and the coefficient of width variation ($C.V._W$) in 0.2079 [3].

As we all know, the simulation and control of crystallization process is possible using the population balance equation (PBE) [4, 5]. Most previous works considered one-dimensional (1D) crystals, and the simulation of crystallization process was successful using the 1D-PBE. However, for many crystals in multi-dimensional (MD) shapes such as needle-like, rod-like, plate-like, polyhedron-like, defining the volume equivalent diameter as the characteristic size seems inadequate. Hence, a more attractive option is to promote the 1D-PBE into the MD-PBE. Through the MD-PBE simulation of crystallization process, the crystal size and shape can be incorporated. In the past 10 years, some authors have reported the application of 2D-PBE [6–8]. For example, Puel *et al* developed a 2D-PBE to simulate the time variation of the length and width of rod-like hydroquinone crystal and solved the 2D-PBE by the discretization method of classes [9, 10]. Ma *et al* presented the modeling of crystallization of potassium dihydrogen phosphate with a shape of a tetragonal prism with two tetragonal bipyramid ends. The 2D-PBE characterized by the width and length of crystal was solved by a hybrid algorithm of the upwind discretization and the Lax-Wendroff method [11]. Ochsenbein *et al* estimated the crystal growth rate of β L-Glutamic acid needles and solved the 2D-PBE by the high resolution method [12]. Oullion *et al* investigated the batch seeded cooling crystallization of a fine organic material, exhibiting a platelet-like habit and designed its time variations of crystal size distribution using the 2D-PBE [13].

Herein, since the $SrCl_2 \cdot 6H_2O$ crystals are in a shape of rod-like, it is reasonable to describe the $SrCl_2 \cdot 6H_2O$ crystal by the length and width of a rectangular parallelepiped and to establish the model of $SrCl_2 \cdot 6H_2O$ growth by the 2D-PBE. In this study, within the above operation range, the model parameters were estimated through fitting the output of 2D-PBE to the experimental 2D-crystals size distribution (CSD) by the method of classes. The modeling of $SrCl_2 \cdot 6H_2O$ growth not only fills the research vacancy of $SrCl_2 \cdot 6H_2O$ crystallization, but also contributes to the optimal control of this crystallization process. That is, the optimal control trajectories can be obtained by simulating the 2D-growth model, which is aimed at a larger size and a narrower size distribution.

2 METHODS

2.1. Experiments

$SrCl_2 \cdot 6H_2O$ of analytical grade was purchased from Sinopharm Chemical Reagent Co. Ltd. (Shanghai, China) and used as received without further purification. Deionized water was used in all the experiments. Different degrees of initial supersaturation and cooling rate were listed in Table 1. An aqueous solution of 600.00 g $SrCl_2$ was added to a 500 mL glass jacketed crystallizer with a flat bottom and equipped with a two-bladed impeller. During the batch process, the impeller was rotated at a fixed speed of 450 rpm. The temperature of the system was controlled using a water bath (PHDC1006, Shanghai Fang Rui Instrument Co., Ltd.) with an accuracy of 0.01 °C and monitored using a thermometer with an accuracy of ± 0.1 °C. The focused beam reflectance measurement (FBRM, Lasentec® S400A, Mettler Toledo, USA) was used to detect

the changes in particle size and number during the crystallization and dissolution. For better information during the crystallization, the operating parameters of the instrument were set as follows, measurement speed: 2 m/s; measurement duration: 2 s; no time averaging; and no weighted chord length.

Table 1. Experiments design for the $SrCl_2 \cdot 6H_2O$ growth rate estimation

Experiment	Initial supersaturation S_0	Cooling rate R (°C·h^{-1})
1	1.163	9.0
2	1.163	12.0
3	1.163	15.0
4	1.163	18.0
5	1.230	9.0
6	1.230	12.0
7	1.230	15.0
8	1.230	18.0

The $SrCl_2$ aqueous solution was first allowed to remain unsaturated for 0.5 h at ~5 °C above T_0 and then linearly cooled to 20.0 °C to start a batch. The initial supersaturation was defined as the ratio of the $SrCl_2$ concentration at T_0 and that at 20.0 °C, according to the solubility data reported

in the literature [14]. The slurry was sampled at the set time-intervals during the cooling. The sample was rapidly centrifugalized to separate crystals from solution. The $SrCl_2 \cdot 6H_2O$ crystals were collected, washed with acetone, and dried in a vacuum oven at 30 °C for 4 h. The crystal phase of this sample was analyzed by the X-ray diffraction (XRD). The XRD patterns were recorded using a diffractometer (D/MAX 2550 VB/PC, Rigaku Co., Tokyo, Japan) equipped with a Cu Kα target radiation source at 40 kV/100 mA operating conditions. The concentration of $SrCl_2$ in the liquid phase was calculated from the Cl^- concentration, which was monitored using a digital titrator (Titrette IT, Brand, Germany) by the $AgNO_3$ titration.

The crystal size of $SrCl_2 \cdot 6H_2O$ were measured using a polarizing microscope (ZEISS Scope A1). Three samples were randomly taken from the $SrCl_2 \cdot 6H_2O$ crystals. From each sample, the crystal length and width of 100 crystals were measured. The size range of 0–2000 μm was equally divided into 200 intervals. For the entire 300 crystals, the number of crystals in each size interval was counted. The size distribution along the length and width directions could be expressed as the Gaussian distribution in Eq. (1) and Eq. (2) [15],

$$n_{L,\%} = \frac{1}{\sqrt{2\pi}\sigma_L} e^{\frac{-(L-L_{mean})^2}{2\sigma_L^2}} \quad (1)$$

$$n_{W,\%} = \frac{1}{\sqrt{2\pi}\sigma_W} e^{\frac{-(W-W_{mean})^2}{2\sigma_W^2}} \quad (2)$$

where $n_{L,\%}$ and $n_{W,\%}$ were the percentage number population densities along the length and width directions, respectively, μm^{-1}; L_{mean} and W_{mean} were the average crystal length and crystal width, respectively, μm; σ_L and σ_W were the standard deviations of crystal length and crystal width, respectively, μm.

The variation coefficient could be calculated by Eq. (3) and Eq. (4) [15],

$$C.V._L = \frac{L_{84\%} - L_{16\%}}{2L_{50\%}} \tag{3}$$

$$C.V._W = \frac{W_{84\%} - W_{16\%}}{2W_{50\%}} \tag{4}$$

where $C.V._L$ and $C.V._W$ were the coefficients of length and width variations, respectively; $L_{16\%}$, $L_{50\%}$, $L_{84\%}$ were the average lengths of crystals accounting for 16%, 50%, 84% of the total measured crystals, respectively, μm; $W_{16\%}$, $W_{50\%}$, $W_{84\%}$ were the average widths of crystals accounting for 16%, 50%, 84% of the total measured crystals, respectively, μm.

As a result, the 2D-CSD of $SrCl_2 \cdot 6H_2O$ could be expressed by Eq. (5),

$$n_{\%}(L,W) = \frac{1}{2\pi\sigma_L\sigma_W}\exp\left[\frac{-(L-L_{mean})^2}{2\sigma_L{}^2} + \frac{-(W-W_{mean})^2}{2\sigma_W{}^2}\right] \tag{5}$$

where $n_{\%}$ was the 2D percentage number population density, μm^{-2}.

The percentage number population ($N_{\%}$) belonging to a certain size range could be calculated by Eq.(6),

$$N_{\%} = \int_L \int_W n_{\%}(L,W,t)dLdW \tag{6}$$

2.2. Modeling of the Two-Dimensional Crystallization Process

The modeling of the unseeded $SrCl_2 \cdot 6H_2O$ batch cooling crystallization was conducted as follows [16]. It was assumed that the CSD did not depend on the spatial coordinates in the well-mixed crystallizer. Besides, the agglomeration and breakage were assumed to be negligible, because no such obvious phenomena were observed during the experiments. Thus, the crystallization could be written by the following equation,

$$\frac{1}{V_T(t)}\frac{\partial}{\partial t}\left[n(L,W,t)V_T(t)\right]+\frac{\partial}{\partial L}\left[G_L(L,t)n(L,W,t)\right] + \frac{\partial}{\partial W}\left[G_W(W,t)n(L,W,t)\right]=r_{N1}+r_{N2} \tag{7}$$

where V_T was the total volume of slurry, m^3; t was the time, s; n was the number population density in the slurry, $\#\cdot\mu m^{-2}\cdot m^{-3}$; G_L and G_W were crystal growth rates along the length and width directions, respectively, $\mu m\cdot s^{-1}$; r_{N1} and r_{N2} were the primary and secondary nucleation rates, respectively, $\#\cdot s^{-1}\cdot m^{-3}$.

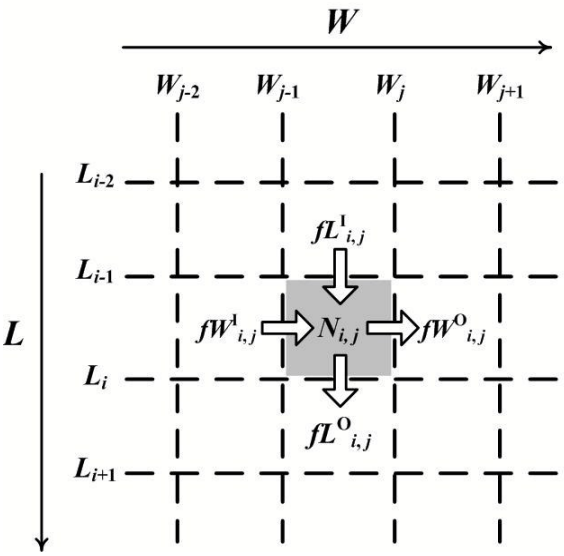

Figure 1. Schematic diagram of the classes method

Here, the 2D-PBE was solved by the method of classes. As shown in Figure 1, the spatial domain of crystal length (L) and width (W) was divided into a system of $im \times jm$ classes, and thus the class $Cl_{i,j}$ was delimited by (L_i, L_{i-1}), (W_j, W_{j-1}). The extents of the class were given by Eq. (8) and Eq. (9) and the characteristic sizes of the class were expressed by Eq. (10) and Eq. (11).

$$\Delta Cl_i = L_i - L_{i-1} \tag{8}$$

$$\Delta Cl_j = W_j - W_{j-1} \tag{9}$$

$$\overline{L_i} = \left(L_{i-1} + L_i\right)/2 \tag{10}$$

$$\overline{W_j} = \left(W_{j-1} + W_j\right)/2 \tag{11}$$

Accordingly, the 2D-PBE around the class $Cl_{i,j}$ led to a set of $im \times jm$ ordinary differential equations (ODEs),

$$\frac{1}{V_T(t)}\frac{d}{dt}\left[N_{i,j}(t)V_T(t)\right] + FL_{i,j}(t) + FW_{i,j}(t) = r_{N1} + r_{N2} \tag{12}$$

with $N_{i,j}(t)$ was the number populations of crystal belonging to the class $Cl_{i,j}$, #·m^{-3}:

$$N_{j1,j2}(t) = N \times \int_{L_{j1-1}}^{L_{j1}} \int_{W_{j2-1}}^{W_{j2}} n_{\%}(L,W,t)\,dL\,dW \tag{13}$$

where N was the number population of crystals in the crystallizer, #·μm^{-2}·m^{-3}.

The net flow, $FL_{i,j}(t)$, of crystals belonging to the class $Cl_{i,j}$ in the length direction could be calculated using the first-order Taylor series expansion Eq.(14), #·s^{-1}·m^{-3},

$$\begin{aligned} FL_{i,j}(t) &= fL^O_{i,j} - fL^I_{i,j} \\ &= G_L\left(\overline{L_i}, t\right)\left[a_i N_{i,j}(t) + b_i N_{i+1,j}(t)\right] - G_L\left(\overline{L_{i-1}}, t\right)\left[a_{i-1} N_{i-1,j}(t) + b_{i-1} N_{i,j}(t)\right] \end{aligned} \tag{14}$$

with

$$a_i = \frac{\Delta Cl_{i+1}}{\Delta Cl_i\left(\Delta Cl_{i+1} + \Delta Cl_i\right)} \tag{15}$$

$$b_i = \frac{\Delta Cl_i}{\Delta Cl_{i+1}\left(\Delta Cl_{i+1} + \Delta Cl_i\right)} \tag{16}$$

where 2 **<** i **<** im-1 and 2 **<** j **<** jm-1.

The net flow, $FW_{i,j}(t)$, of crystals belonging to the class $Cl_{i,j}$ in the width direction could be

calculated in the same way, #·s^{-1}·m^{-3},

$$\begin{aligned} FW_{i,j}(t) &= fW_{i,j}^{O} - fW_{i,j}^{I} \\ &= G_W\left(\overline{W_j},t\right)\left[c_j N_{i,j}(t) + d_j N_{i,j+1}(t)\right] - G_W\left(\overline{W_{j-1}},t\right)\left[c_{j-1} N_{i,j-1}(t) + d_{j-1} N_{i,j}(t)\right] \end{aligned} \tag{17}$$

with

$$c_j = \frac{\Delta Cl_{j+1}}{\Delta Cl_j\left(\Delta Cl_{j+1} + \Delta Cl_j\right)} \tag{18}$$

$$d_j = \frac{\Delta Cl_j}{\Delta Cl_{j+1}\left(\Delta Cl_{j+1} + \Delta Cl_j\right)} \tag{19}$$

where 2 **<** *i* **<** *im*-1 and 2 **<** *j* **<** *jm*-1.

The crystal flows corresponding to the boundary classes were considered and expressed by the following equations,

$$fL_{1,j}^{inlet}(t) = fW_{i,1}^{inlet}(t) = 0 \tag{20}$$

$$fL_{im,j}^{outlet}(t) = fW_{i,jm}^{outlent}(t) = 0 \tag{21}$$

Moreover, the mass balance during the unseeded $SrCl_2 \cdot 6H_2O$ batch cooling crystallization was required and was expressed by Eq.(22),

$$d\left[V(t)C(t) + V_T(t)C_S(t)\right]/dt = 0 \tag{22}$$

where $V(t)$ was the total volume of solution, m^3; $C(t)$ was the solute concentration, mol·m^{-3}; $C_S(t)$ was the solid concentration, mol·m^{-3}.

For a well-mixed batch crystallizer, $C_S(t)$ could be computed from the 2D-CSD at a given time by Eq.(23),

$$C_S(t) = \frac{\rho_S}{M_S} \times N \times \int_L \int_W LW^2 \times n_{\%}(L,W,t) dL dW \tag{23}$$

where ρ_S was the $SrCl_2 \cdot 6H_2O$ density, 1930 $kg \cdot m^{-3}$; M_S was the $SrCl_2 \cdot 6H_2O$ molar mass, 0.26662 $kg \cdot mol^{-1}$. Considering the negligible effects of crystallization and temperature variation on the total solution volume, the total volume of slurry($V_T(t)$) could be computed by Eq.(24),

$$V_T(t) = V(0) \Big/ \left(1 - \frac{M_S}{\rho_S} C_s(t)\right) \tag{24}$$

where $V(0)$ was the initial total volume of solution, m^3.

Thus, the number population of crystals in the crystallizer, N, could be calculated by Eq.(25),

$$N = \frac{C(0) - C(t) \Big/ \left[\frac{\rho_S}{M_S} + (C(0) - C(t))\right]}{\int_L \int_W LW^2 \times n_{\%}(L, W, t) dL dW} \tag{25}$$

3 RESULTS AND DISCUSSION

3.1. Mechanism of the $SrCl_2 \cdot 6H_2O$ Growth. Figures 2 and 3 illustrated the variations of solute concentration, superaturation, and crystal size during the experiments. When the temperature decreased, supersaturation accumulated until a burst nucleation occurred. Numerous crystal nucleuses emerged and consumed the solute. Consequently, the supersaturation decreased quickly. However, a large amount of new-born crystal nucleuses dissolved again due to a short heating-up in system caused by this exothermic crystallization process. Afterwards, since the cooling profile was never stopped, the system temperature would sequentially decrease. The existing crystal nucleuses went on growing up, and both the crystal length and width increased rapidly. As the supersaturation in system was continuously consumed, the growth rate of crystals gradually decreased until the end of the cooling profile.

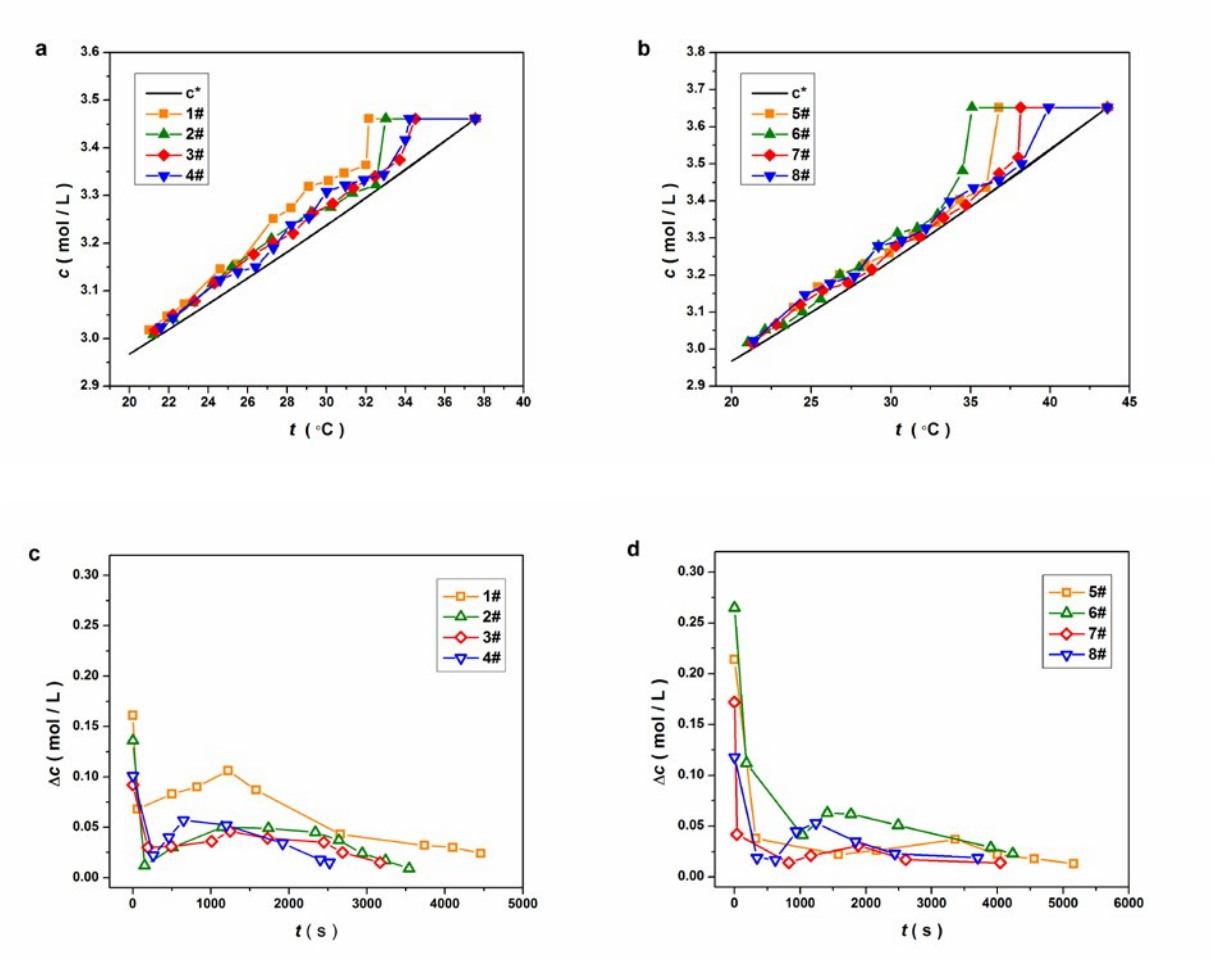

Figure 2. Variations of solute concentration (a, b) and supersaturation (c, d) during experiments

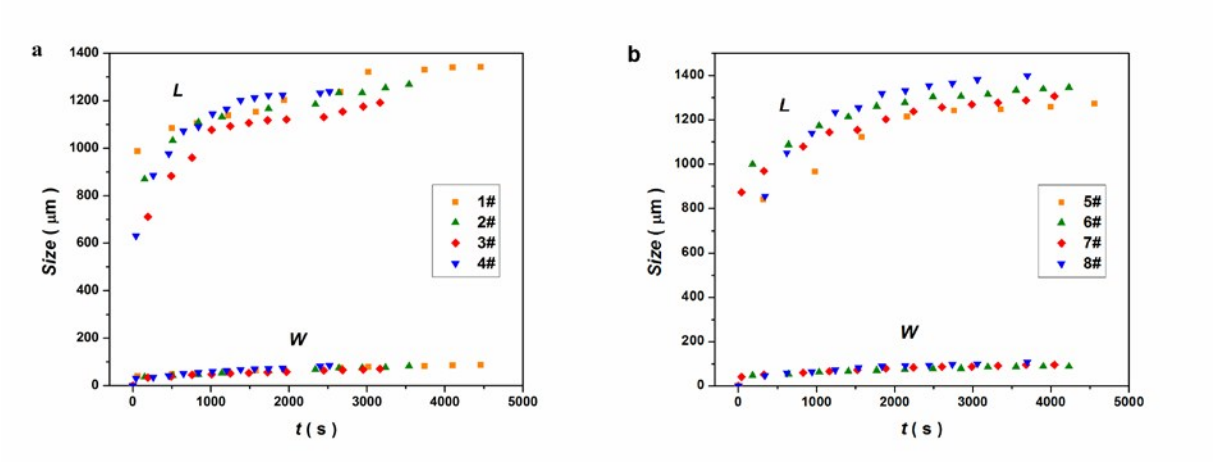

Figure 3. Variation of crystal size during experiments

For example, in Experiment 3, the on-line monitoring of the crystallization process was shown in Figure 4. Driven by the external forced cooling profile, the regulation of the amount of crystal nucleuses completed very soon. The gradual right-moving chord-length distribution (CLD) peak revealed that the undissolved crystal nucleuses grew up by consuming the supersaturation in system. The maintained n_c (chord counts) value proved that no obvious agglomeration and breakage were observed. In this exact period we discussed, these undissolved crystal nucleuses just acted as the seed crystals. They adsorbed solute and went on growing up. Thus, the growth process of these undissolved crystal nucleuses could be regarded as a lightly seeded batch cooling crystallization process [17]. To a certain extent, it was acceptable to assume that there is no significant primary and secondary nucleation. So the 2D-PBE in Eq. (12) could be written as follows:

$$\frac{1}{V_T(t)}\frac{d}{dt}\left[N_{i,j}(t)V_T(t)\right]+FL_{i,j}(t)+FW_{i,j}(t)=0 \tag{26}$$

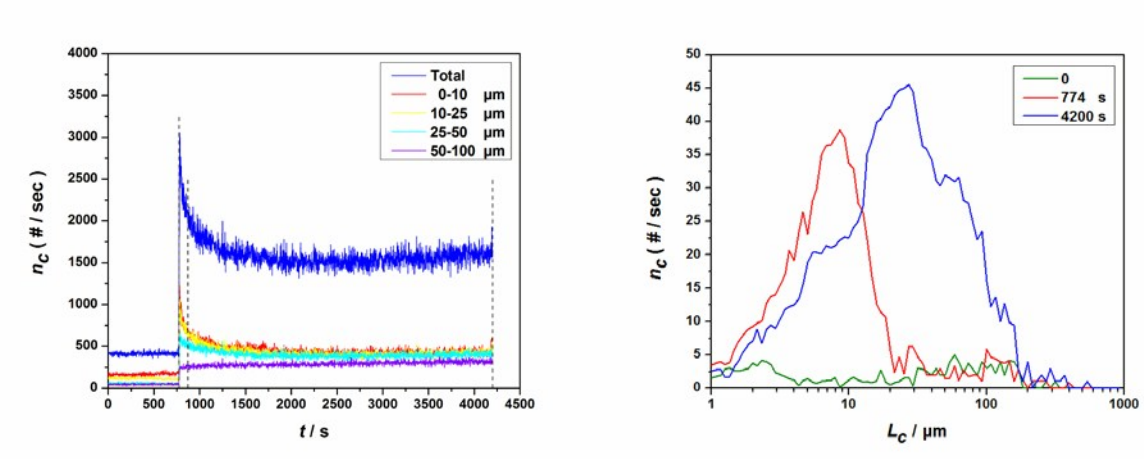

Figure 4. On-line monitoring of the $SrCl_2 \cdot 6H_2O$ crystallization process

Furthermore, a prominent broadening of the 2D-CSD in this discussed period at 892 s, 1088 s, 1488s, and 2952 s was demonstrated in Figure 5. It additionally turned out a size dependent growth mechanism of $SrCl_2 \cdot 6H_2O$, which made the size difference becoming greater and greater.

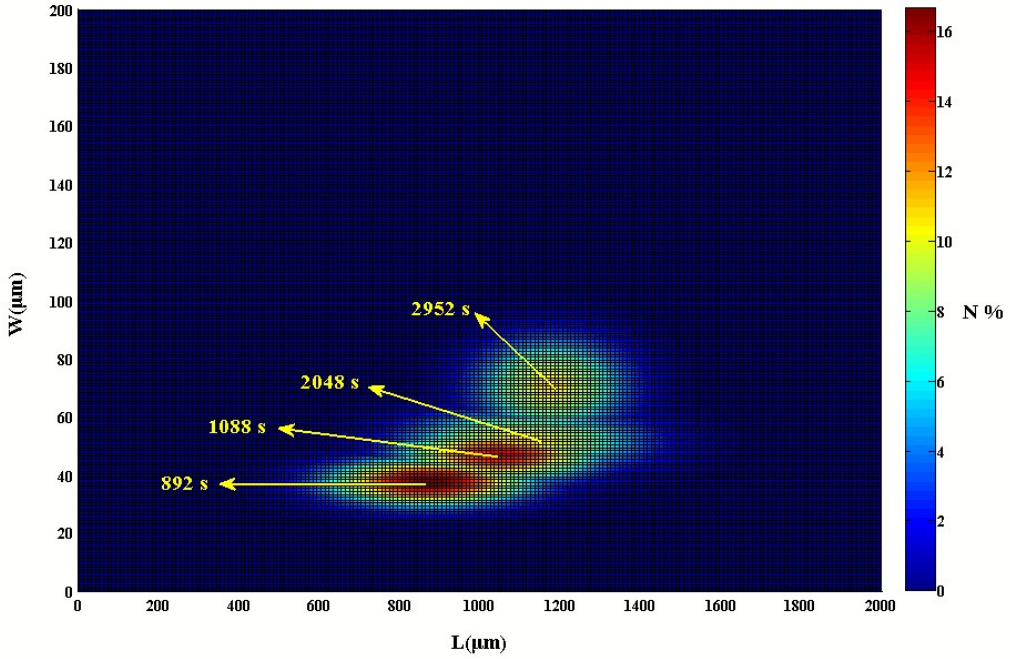

Figure 5. Variation of crystal size and size distribution during the $SrCl_2 \cdot 6H_2O$ crystallization process

3.2. Establishment of the $SrCl_2 \cdot 6H_2O$ Growth Model. The crystal growth rate can either be limited by mass transfer or by the integration of solute into the crystal surface. In the case of $SrCl_2 \cdot 6H_2O$ crystals, growth is considered to be surface integration controlled within the investigated operation range, as concluded in our previous study that the stirring rate played a less significant role on the crystal size and size distribution [3]. Two dominating mechanisms

"birth and spread" [18] and "screw dislocations" [19] were identified for this surface-integration-controlled growth. The typical 50× and 100× microscope images of $SrCl_2 \cdot 6H_2O$ sample were shown in Figure 6. The crystal surfaces were smooth without any spiral ripples, indicating a "birth and spread" mechanism of the $SrCl_2 \cdot 6H_2O$ growth at a relatively low supersaturation [20].

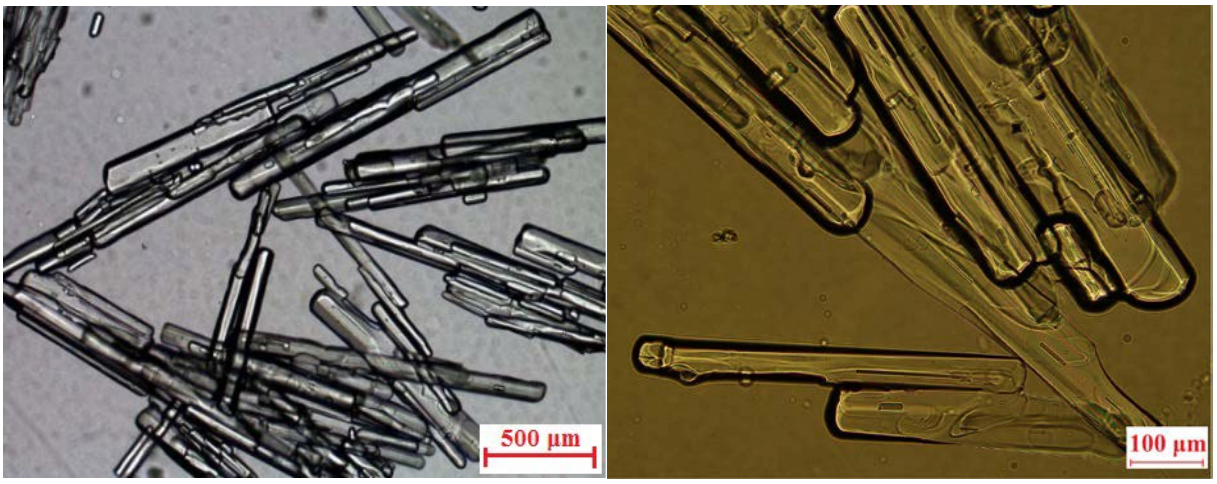

Figure 6. Microscope image of the $SrCl_2 \cdot 6H_2O$ sample

Therefore, in this study, the $SrCl_2 \cdot 6H_2O$ growth rate model was built from the combination of two base expressions: a mechanistic "birth and spread" (B) type expression [9, 19] in Eq. (27) and a purely empirical (E) type in Eq.(28) [21, 22]:

$$G = p_1 \exp\left(-\frac{p_2}{T^2 \ln(S)}\right) \exp\left(-\frac{p_3}{T}\right) (S-1)^{2/3} (\ln S)^{1/6} \quad (27)$$

$$G = p_1 (S-1)^{p_2} \exp\left(-\frac{p_3}{T}\right) \quad (28)$$

where G was the growth rate, $\mu m \cdot s^{-1}$; S was the supersaturated ratio; T was the temperature, K; p_1,

p_2, p_3 were the model parameters.

Besides, the $SrCl_2 \cdot 6H_2O$ growth followed a size dependent growth mechanism. To this end, the growth rate model was extended to include a simple power law dependency expressed by the Eq. (29) and Eq. (30) [9]:

$$G_L = G^{B/E} \times L^{p_{4,i}} \tag{29}$$

$$G_W = G^{B/E} \times W^{p_{4,j}} \tag{30}$$

where G_L and G_W were the growth rate along the length and width directions, μm·s^{-1}; L and W were the crystal length and width, μm; $p_{4,i}$ and $p_{4,j}$ were the model parameters.

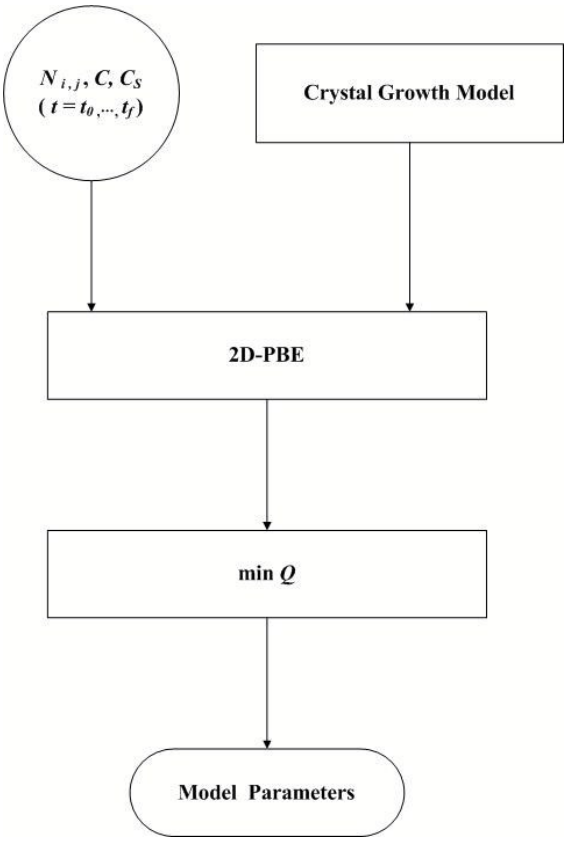

Figure 7. Parameters estimation of the $SrCl_2 \cdot 6H_2O$ growth rate model

3.3. Model Solution and Verification. As shown in Figure 7, the model parameters estimation was performed by fitting the output of the simultaneous mass balance equation (Eq. (22)), 2D-PBE (Eq. (26)) and $SrCl_2 \cdot 6H_2O$ growth model(Eq. (29) and Eq. (30)) to the experimental data of 2D-CSD and the solute concentration at different time in the discussed period.

The spatial domain of crystal length (L=0–2000 μm) and width (W=0–200μm) was divided into a system of 20×20 classes, 200×20 classes, 200×200 classes, respectively. Also taking the Experiment 3 for example, at 892 s, the accuracy of numerically calculated classes was studied by comparing the calculated CSD with the experimental data [23], as listed in Table 2. A reasonable accuracy was obtained under the classes of 200×200. Thus, comprehensively considering the calculation accuracy and time, the number of classes was not added continuously, and the classes of 200×200 were used here.

Table 2. Comparison of the experimental CSD with the calculated CSD under different classes

CSD	Experimental	20×20 Classes	200×20 Classes	200×200 Classes
L_{mean} (μm)	868.36	867.91	868.36	868.36
σ_L (μm)	171.32	174.37	170.41	170.41
W_{mean} (μm)	37.23	36.79	36.79	37.23
σ_W (μm)	5.56	6.97	6.97	5.55

The model parameters estimation was done by seeking the maximum likelihood estimate

(MLE), which could be regarded as the minimization of the following function:

$$Q = \left[\frac{1}{V_T(t)} \frac{d}{dt} \left(N_{i,j}(t) V_T(t) \right) + FL_{i,j}(t) + FW_{i,j}(t) - 0 \right]^2 \quad (31)$$

The minimization of Eq. 31 was actually a nonlinear optimization problem. To obtain a global optimization, the genetic algorithm was run by using the GA toolbox in Matlab 7.10.0 R2012a to seek the initial values for the local optimizer and ended when the genetic generation and the stall generation limit reached to 1000 and 300, respectively. The function *fminunc* implemented in the optimization toolbox in Matlab 7.10.0 R2012a was applied for the local optimization. When the maximum time for function evaluation reached to 200, the run was ended and the final solution was obtained.

The resulting fit was given by the following equations, where each model was expressed with eight parameters:

$$G_L = 0.2143 \exp\left(-\frac{0.6942}{T^2 \ln(S)} \right) \exp\left(-\frac{0.9601}{T} \right) (S-1)^{2/3} (\ln S)^{1/6} \times L^{0.4094} \quad (32a)$$

$$G_W = 0.0003 \exp\left(-\frac{0.5356}{T^2 \ln(S)} \right) \exp\left(-\frac{0.4319}{T} \right) (S-1)^{2/3} (\ln S)^{1/6} \times L^{1.9037} \quad (32b)$$

The model verification was illustrated in Figure 8. On one hand, the reproducibility of the model was needed to be verified. For all eight experiments, the comparisons of the experimental and calculated solute concentration and 2D-CSD were shown in Figures 9 and 10. It could be found that, the calculated outputs followed the measured data in a satisfactory manner for each experiment. Despite a little offset in the standard deviation of crystal length, the calculated points lied nearly in the both sides of the experimental curve, and the variation trends were consistent.

On the other hand, the predictability of the model was needed to be verified. Here, an additional batch-cooling crystallization process was discussed, under an initial supersaturation of 1.200, a cooling rate of 12.80 °C·h^{-1} and a stirring rate of 450 rpm. The comparisons of the experimental and calculated solute concentration and 2D-CSD were shown in Figures 11 and 12. Also, the calculated outputs were found to satisfactorily agree with the measured data. The mean relative errors (MRE) of the above 9 experiments were listed in Table 3. The corresponding MREs in the solute concentration, crystal size, and size distribution were less than 1%, 10%, and 15%, respectively.

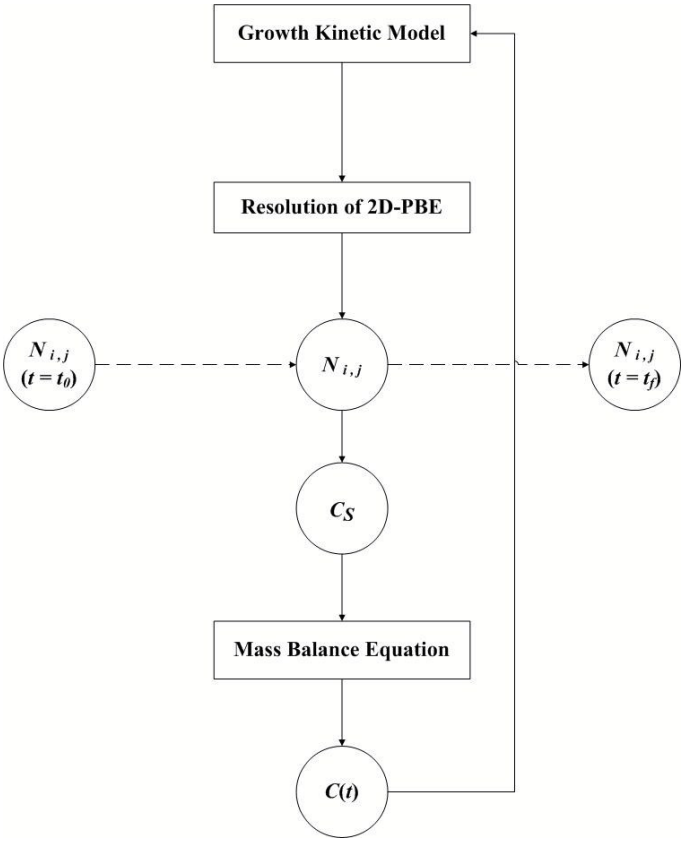

Figure 8. Verification of the $SrCl_2 \cdot 6H_2O$ growth rate model

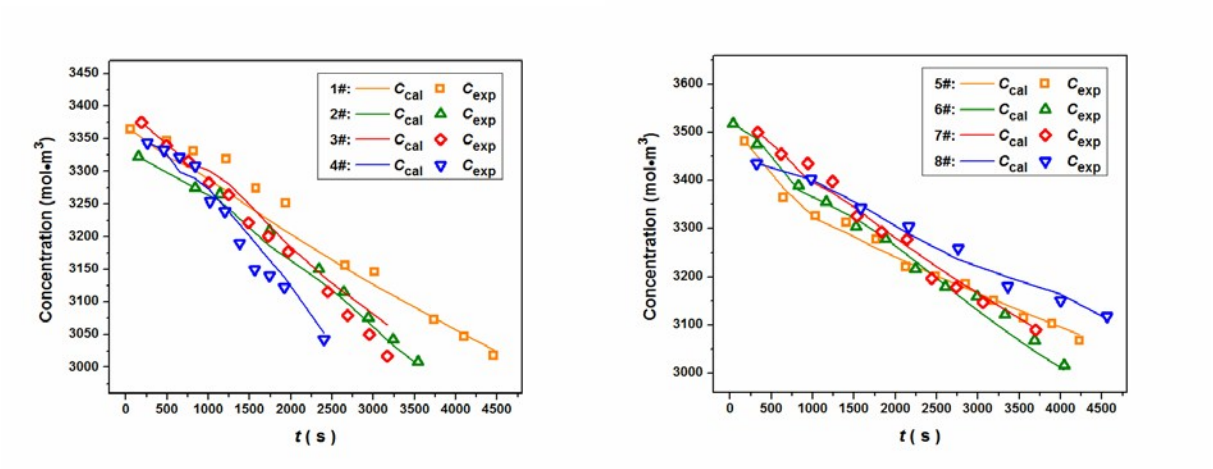

Figure 9. Reproducibility verification of solute concentration

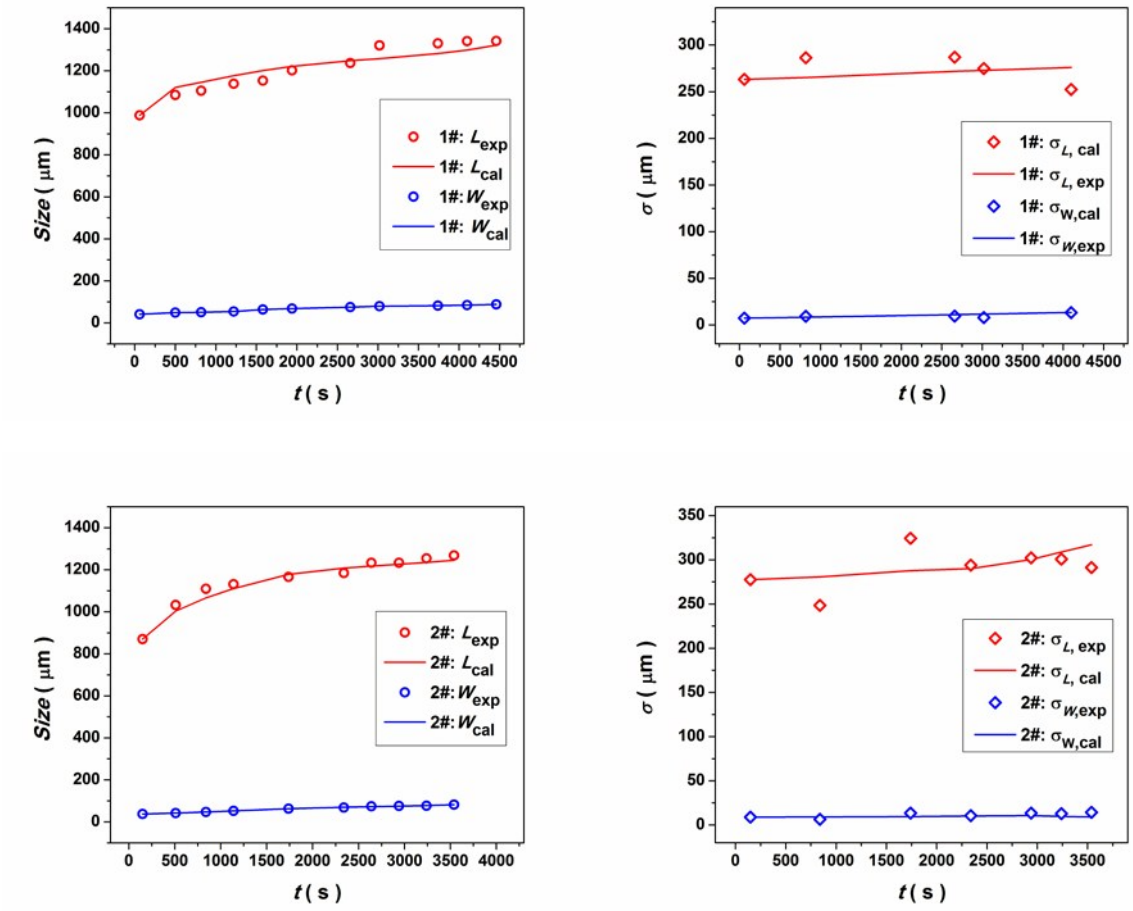

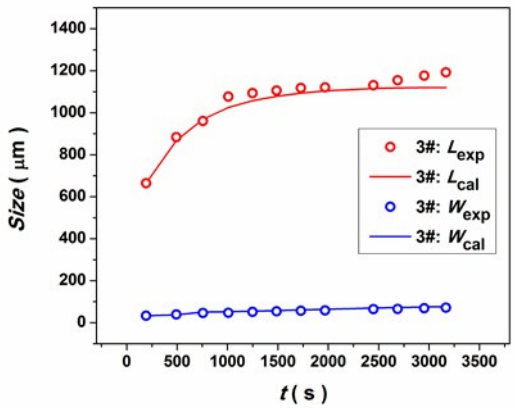

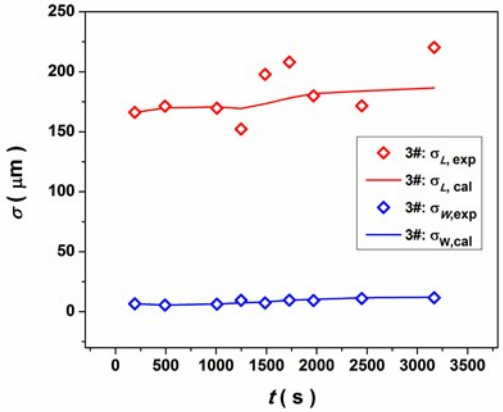

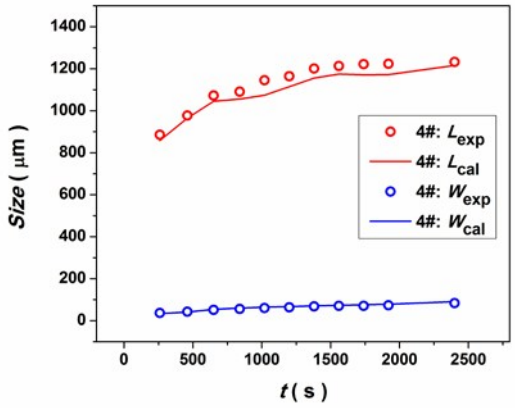

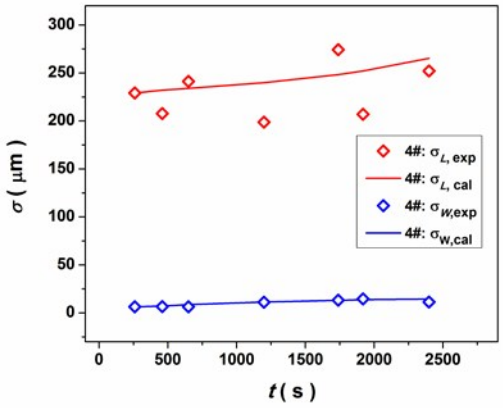

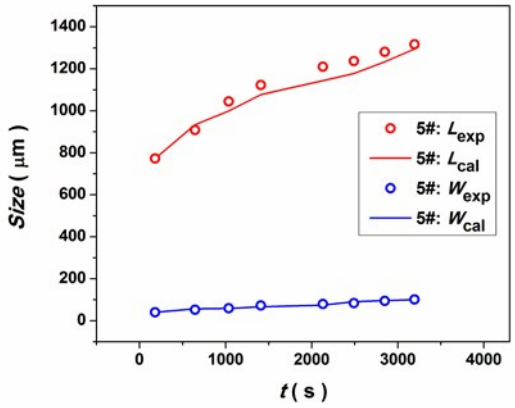

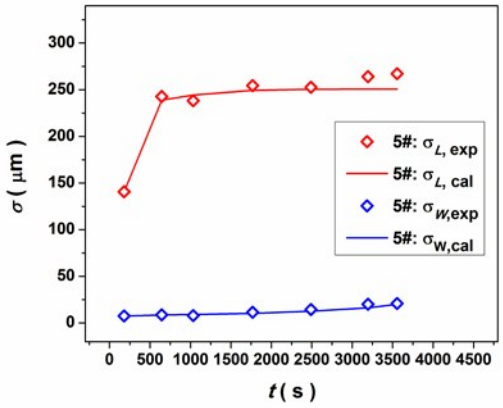

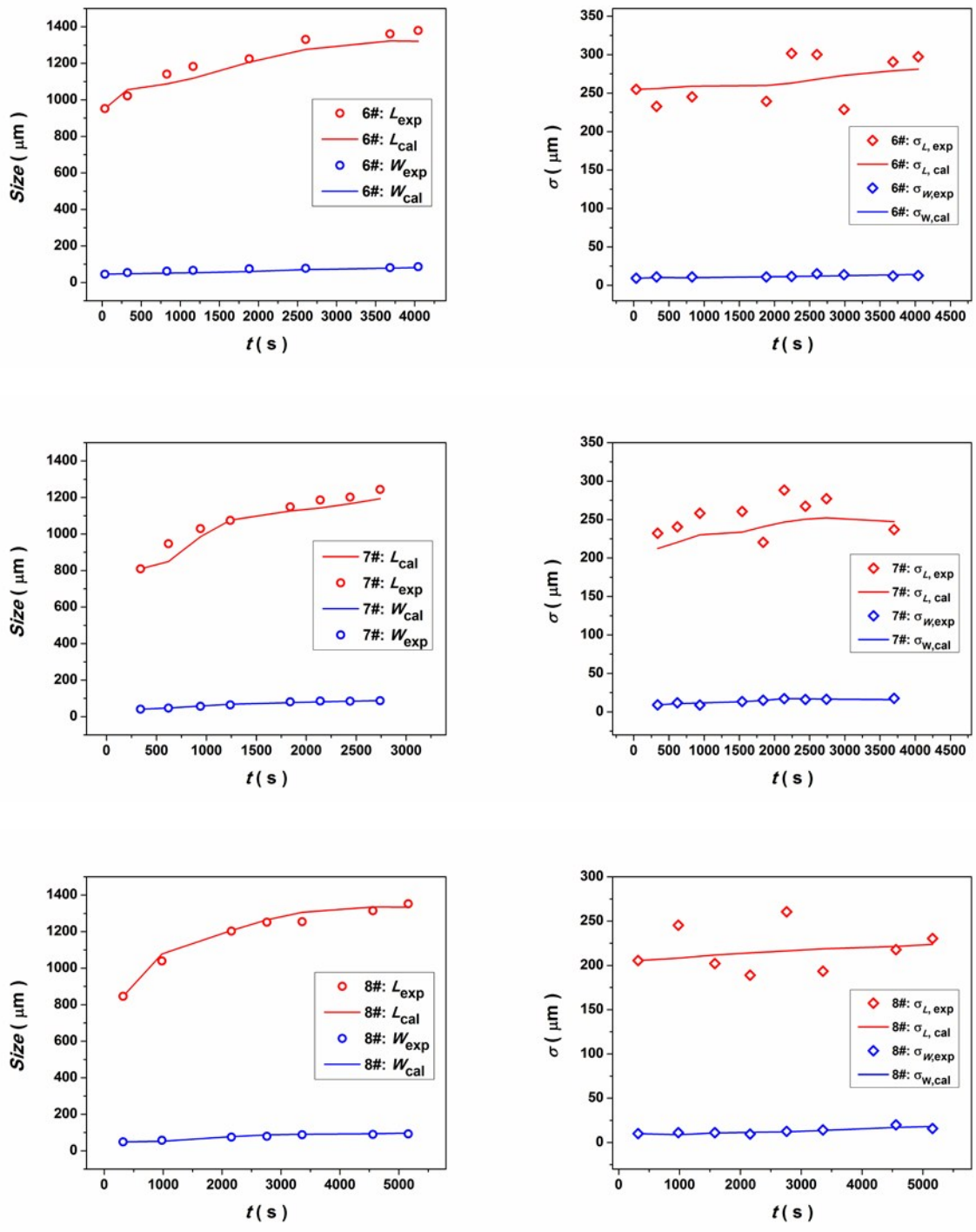

Figure 10. Reproducibility verification of crystal mean size and size distribution

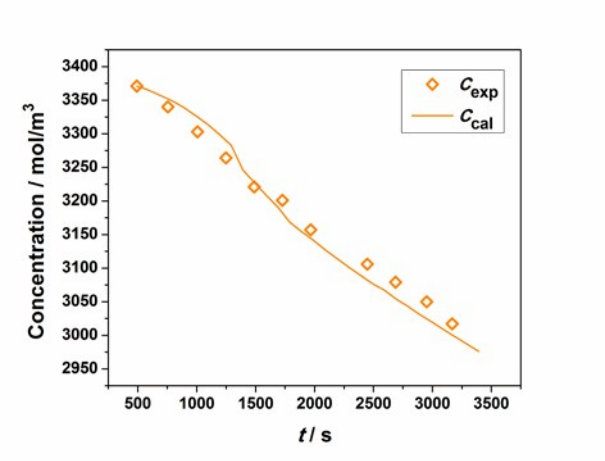

Figure 11. Predictability verification of solute concentration

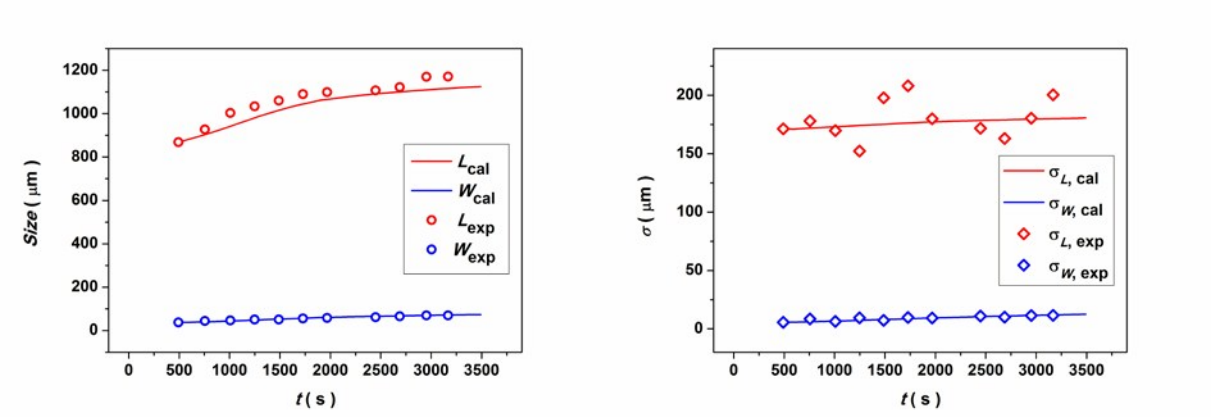

Figure 12. Predictability verification of crystal mean size and size distribution

Besides, the results of XRD analysis on the crystals, sampled from the above 9 experiments, indicated that all of them were pure $SrCl_2 \cdot 6H_2O$. For conciseness reasons, the typical XRD pattern was given in Figure 13.

Generally, within a best operational range given as an initial supersaturation of 1.150~1.250, a cooling rate of 15.0~20 °C·h^{-1}, a stirring rate of 450 rpm and an aging time of 10 min [3], the

$SrCl_2 \cdot 6H_2O$ growth model (Eq. (32)) could well describe the growth behavior of $SrCl_2 \cdot 6H_2O$ in the system.

Table 3. Mean relative errors of the fitting using the $SrCl_2 \cdot 6H_2O$ growth rate model

No.	MRE_c (%)	MRE_L (%)	$MRE_{\sigma L}$ (%)	MRE_W (%)	$MRE_{\sigma W}$ (%)
1	0.67	2.99	5.70	6.81	8.85
2	0.32	1.85	5.80	6.03	10.59
3	0.67	3.06	7.87	8.40	6.85
4	0.52	3.38	10.27	6.06	11.04
5	0.32	3.85	6.05	5.37	10.28
6	0.44	3.74	10.16	7.31	8.90
7	0.82	3.92	8.99	3.08	7.39
8	0.37	2.02	9.69	5.46	11.76
predictability verfication	0.28	1.45	5.20	4.43	6.13

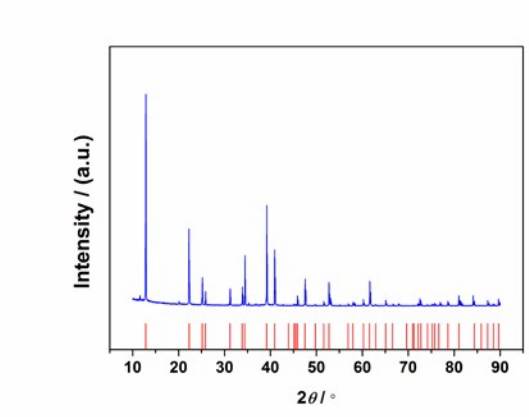

Figure 13. XRD pattern of the typical crystals sample. The red vertical lines denote the positions of diffraction peaks in the standard JCPDS 06-0073 of $SrCl_2 \cdot 6H_2O$.

4 Conclusion

The growth of strontium chloride hexahydrate during unseeded batch cooling crystallization was investigated and modeled by the two-dimensional population balance equation.

In a well-mixed crystallizer, no obvious agglomeration and breakage were observed. The initial supersaturation and cooling rate were the key factors of crystal growth, whereas stirring rate and aging time were undistinguished factors. During the batch-cooling crystallization process, a quick regulation of the amount of crystal nucleuses occurred after a burst nucleation, due to a short heating-up in system caused by the exothermic crystallization process. Then, the rest crystal nucleuses went on growing up forced by the non-stopped cooling profile and this growth followed a size dependent mechanism. Therefore, the growth of $SrCl_2 \cdot 6H_2O$ was modeled as a function of supersaturation, temperature, and crystal size. The model parameters were estimated by the method of classes, through fitting the output of the simultaneous 2D-PBE, mass balance equation and $SrCl_2 \cdot 6H_2O$ growth model to the experimental data of 2D-CSD and the solute concentration. The resulting fit was given by a model with eight parameters and the model verification showed that the calculated solute concentration and 2D-CSD matched with the measured data in a satisfactory manner. The corresponding MREs in the solute concentration, crystal size, and size distribution were less than 1%, 10%, and 15%, respectively. In generally, the model could well predict the growth behavior of $SrCl_2 \cdot 6H_2O$ in the system.

This study not only fills the research vacancy of $SrCl_2 \cdot 6H_2O$ crystallization, but also contributes to the optimal control of this crystallization process. That is, the optimal control trajectories can be obtained by simulating the 2D-growth model, which is aimed at a larger size and a narrower size distribution.

Acknowledgements

This work was financially supported by the Fundamental Research Funds for the Central Universities.

Notes and references

[1] Z. Cheng, Y. Chang and L. Wang, *Inorg. Chem. Ind.* 2010, **42**, 46.

[2] L. Wei, Y. Wang and Z. Sha, *J. Salt Chem. Ind.* 2010, **39**, 26.

[3] Y. Y. Qian, G. M. Lu, Y. Z. Sun, X. F. Song and J. G. Yu, *Cryst. Res. Technol.* 2014, **49**, 878

[4] H. M. Hulburt and S. Katz, *Chem. Eng. Sci.* 1964, **19**, 555.

[5] A. D. Randolph and M. A. Larson, *Theory of particulate processes*, Academic Press, San Diego, 1988.

[6] A. Gerstlauer, A. Mitrovic and S. Motz, *Chem. Eng. Sci.* 2001, **56**, 2553.

[7] H. Briesen, *Chem. Eng. Sci.* 2006, **61**, 104.

[8] D. Rmakrishna and A. W. Mahoney, *Chem. Eng. Sci.* 2002, **57**, 595.

[9] F. Puel, G. Fevotte and J. P. Klein, *Chem. Eng. Sci.* 2003, **58**, 3715.

[10] F. Puel, G. Fevotte and J. P. Klein, *Chem. Eng. Sci.* 2003, **58**, 3729.

[11] D. L. Ma, D. K. Tafti and R. D. Braatz, *Ind. Eng. Chem. Res.* 2002, **41**, 6217.

[12] D. R. Ochsenbein, S. Schorsch, T. Vetter, M. Mazzotti and M. Morari, *Ind. Eng. Chem. Res.* 2013, **53**, 9136.

[13] M. Oullion, F. Puel, G. Fevotte, S. Righini and P. Carvin, *Chem. Eng. Sci.* 2007, **62**, 833–845.

[14] Y. Y. Qian, G. M. Lu, Y. Z. Sun, X. F. Song and J. G. Yu, *Cryst. Res. Technol.* 2014, **49**, 78.

[15] H. X. Ding and S. Tan, *Industrial Crystallization*, Chemical Industry Press, Beijing, 1985.

[16] C. Y. Ma, X. Z. Wang and K. J. Roberts, *Adv. Powder Technol.* 2007, **18**, 707.

[17] D. C. Huang, Z. X. Wang, W. Liu and Y. M. Sun, *Acta Chimica Sinica*, 2006, **64**, 611.

[18] M. Ohara and R. C. Reid, *Modeling crystal growth rates from solution*, Prentice Hall Inc., Englewood Cliffs, 1973.

[19] W. K. Burton, N. Cavrera and F. C. Frank, *Philos. Trans. R. Soc.* 1951, **243**, 299.

[20] J. W. Mullin, *Crystallization (3rd Edition)*, Butterworth Heinemann Press, Oxford, 1992.

[21] J. Scholl, C. Lindenberg, L. Vicum and M. Mazzotti, *Faraday Disc.* 2007, **136**, 247.

[22] M. Kitamura and T. Ishizu, *J. Cryst. Growth.* 2000, **209**, 138.

[23] L. Shaikh, A. Pandit and V. Ranade, *Can. J. Chem. Eng.* 2013, **91**, 47.

The growth of strontium chloride hexahydrate during unseeded batch cooling crystallization was modeled by the two-dimensional population balance equation.